

Spectral Filters, Dark Signals, and Attention Sinks

Nicola Cancedda

FAIR at Meta

Projecting intermediate representations onto the vocabulary is an increasingly popular interpretation tool for transformer-based LLMs, also known as the *logit lens* (Nostalgebraist). We propose a quantitative extension to this approach and define *spectral filters* on intermediate representations based on partitioning the singular vectors of the vocabulary embedding and unembedding matrices into bands. We find that the signals exchanged in the tail end of the spectrum are responsible for attention sinking (Xiao et al., 2023), of which we provide an explanation. We find that the loss of pretrained models can be kept low despite suppressing sizeable parts of the embedding spectrum in a layer-dependent way, as long as attention sinking is preserved. Finally, we discover that the representation of tokens that draw attention from many tokens have large projections on the tail end of the spectrum.

Date: February 15, 2024

Correspondence: Nicola Cancedda at ncan@meta.com



1 Introduction

Large foundation models dominate the state of the art in numerous AI tasks. While we understand how these models work in terms of elementary operations, and black-box evaluations help characterize observable behaviours, we lack a clear understanding of the connection between the two.

There is a growing body of work providing insights into properties of model components, e.g. (Voita et al., 2019; Pimentel et al., 2020; Voita and Titov, 2020; Geva et al., 2022; Meng et al., 2022; Voita et al., 2023), as well as identifying and explaining fundamental phenomena, often with the support of simple models (Elhage et al., 2021, 2022; Olsson et al., 2022; Todd et al., 2023).

Most recent works assign a central role to the model’s *residual stream* (RS) as the shared communication channel between model components. In this perspective, the probability distribution of a token is initialised from the projection of the embedding of the previous token through the unembedding matrix, and receives additive updates from attention heads and MLP components, each reading from the residual stream of the same or previous tokens. The role played by components is interpreted projecting their contribution on the probability distribution over vocabulary items, in what is referred to as the *logit lens* (Nostalgebraist; Geva et al., 2020). We extend this approach and introduce *logit spectroscopy*, the

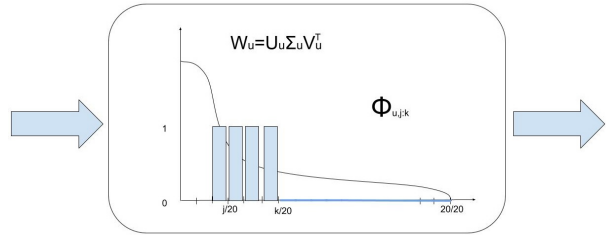


Figure 1 Spectral filters project signals exchanged between components onto selected subspaces as defined by the spectral decomposition of the vocabulary embedding and unembedding matrices of the model.

spectral analysis of the content of the residual stream and of the parameter matrices interacting with it. Equipped with this tool, we look at the part of the residual stream spectrum that is most likely to be neglected by the logit lens: the linear subspace spanned by the right singular vectors of the unembedding matrix with the *smallest* singular values. Drawing an analogy with “dark matter” in astrophysics, that interacts with light only indirectly, we dub projections onto this subspace *dark* parameters, features, activations etc.

We were motivated by the thought that LLMs could learn to use signals in the dark linear subspace to maintain global features responsible for long-range dependencies while minimizing their interference with the next token prediction. We discovered instead that

dark signals are instrumental to implementing the recently described phenomenon of *attention sinks* (Xiao et al., 2023), of which we provide a detailed account. We also show that the negative log likelihood of pre-trained models can be kept low despite suppressing large swaths of the unembedding spectrum, as long as the dark signals required for attention sinking are untouched. Finally, we find a significant positive correlation between the average attention received by a token and the relative prevalence of dark signals in its residual stream.

2 The LLaMa2 models

We chose LLaMa2 models (Touvron et al., 2023) as the object of our study as they were the most competitive models with open-access weights at the time we started this work. In particular we studied pretrained models (without instruction fine-tuning) with 7B, 13B, and 70B parameters.

Table 1 presents the key dimensional hyperparameters of these models. All LLaMa2 models share the same tokenizer, with 32,000 vocabulary items. Table 3, in Appendix A, summarizes the standard notation we use to refer to model components.

We point out a few differences between LLaMa2 models and the original transformer architecture (Vaswani et al., 2017). RMSnorm (Zhang and Senrich, 2019) is applied *before* every attention component, MLP component, and the final unembedding projection. RMSnorm includes a learned rescaling vector that is applied after the normalization proper. In all cases, we absorb this rescaling vector into the matrices downstream from the rescaling: this is mathematically equivalent and simplifies the analysis.

LLaMa2 models use SwiGLU activation functions (Shazeer, 2020):

$$\begin{aligned} \text{FFN}_{\text{SwiGLU}}(x, W_1, W_2, W_3) & \\ &= (\text{Swish}_1(xW_1) \otimes xW_3)W_2 \end{aligned} \quad (1)$$

This means that MLP components have three parameter matrices instead of the more familiar two.

Finally, LLaMa2 models use rotary positional embeddings (Su et al., 2023). While important for the functioning of the model, their effect is independent of the phenomena we are focusing on.

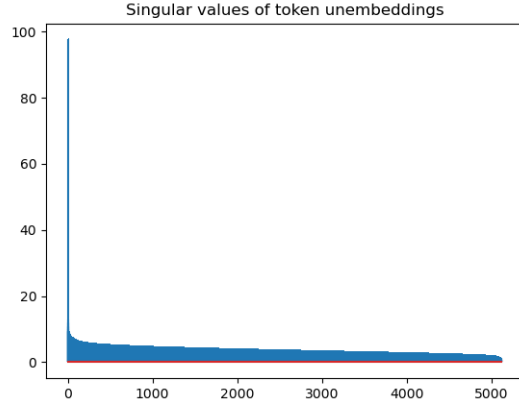


Figure 2 Distribution of the singular values of the unembedding matrix W_u of LLaMa2 13B. The *U-Dark* subspace is the one spanned by the last 5% right singular vectors.

3 Model parameter properties

Let $W_u = U_u \Sigma_u V_u^\top$ be the singular value decomposition of the vocabulary unembedding matrix (and similarly for W_e). Figure 2 shows the distribution of the singular values (SVs) of W_u for LLaMa2 13B. There is a single large SV^1 followed by a tail that declines only at the very end (the distribution for LLaMa2 7B and LLaMa2 70B is similar). The SV distribution of the W_e embedding matrix is also similar, but the top SV is only twice as large as the second one, with a longer “head” of relatively large SVs.

We use the adjective *U-dark* (*E-dark*) to characterize anything that happens in the linear subspace spanned by the 5% right singular vectors (RSVs) of W_u (W_e) with the smallest SVs, the dark basis.

We gain an initial insight into whether dark signals are exchanged by projecting rows and columns of parameter matrices on the dark bases. W_k , W_q , and W_v project the residual stream onto either the latent space used to compute attention scores or the latent space used to compute the attention output, so they “read” from the residual stream; similarly W_1 and W_3 map from the residual stream onto the activation layer of the MLP components. We project the columns of these matrices on the RSVs of W_u to estimate and visualize their aptitude to read from the dark subspace². Conversely, W_o and W_2 map from latent spaces back into the residual stream, therefore

¹Projecting unembeddings on the first singular vector shows that it is highly representative of token frequency.

²We adopt the convention that input vectors are row vectors and are multiplied by parameter matrices on the right.

Model	Layers	RS dim	MLP dim	Attn heads	KV heads
LLaMa2 7B	32	4096	11008	32	32
LLaMa2 13B	40	5120	13824	40	40
LLaMa2 70B	80	8192	14336	64	8

Table 1 Dimensional hyper-parameters of the LLaMa2 models. The 70B model uses grouped-query attention, with 64 attention heads sharing 8 key and value matrices.

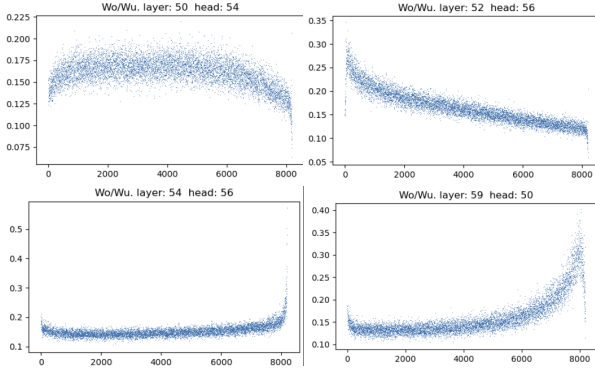


Figure 3 The projections of four W_o matrices of LLaMa2 70B on the RSVs of W_u . Different heads are equipped to write into different subspaces, with some targeting the dark subspace.

we project their rows to check their aptitude to write into the dark subspace. We computed and plotted the norms of the d vectors of dimension d_h or d_m obtained with these projections, e.g.:

$$j_i = \begin{cases} \|(V_u^\top)_i W_y\|_2, & y \in \{k, q, v, 1, 3\} \\ \|(V_u^\top)_i W_y^\top\|_2, & y \in \{o, 2\} \end{cases} \quad (2)$$

We discovered a great variety in where, in the bases formed by the RSVs of W_u and W_e , model components are equipped to read from and write into. Figure 3 gives a sense of such variety.

The projections of MLP matrices also clearly indicate that some MLP components can write mostly into the dark subspace (see Fig.4 for the projection of 13B/L0/ W_2 on W_u).

There are therefore components that are equipped for communicating through the dark subspace. In the following section we explore if such communication actually takes place and how it manifests itself.

4 Spectral filtering

One possible explanation for the existence of components that communicate through the dark subspace is that they are useless, and the model learned to

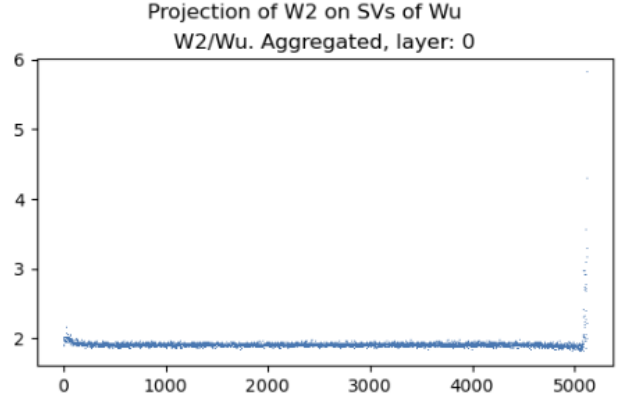


Figure 4 The projection of the rows of W_2 at L0 of LLaMa2 13B on the RSVs of W_u . Note the large values at the very right end of the spectrum, indicating the ability to write in the U-Dark space.

divert their output to subspaces with little bearing on the vocabulary logits. To see if this is the case, we perform a series of experiments, where we patch some of the intermediate representations by projecting them onto the RSVs of W_u and W_e with largest singular vectors, therefore removing dark signals. We measure the average negative log-likelihood (NLL) of tokens in a sample of prompts: if dark signals are irrelevant noise then we expect NLL to be largely unaffected when they are filtered out.

We split the singular vectors of W_u into 20 *bands*: $\{V_{u,1}, \dots, V_{u,20}\}$, of cardinality $d/20$, and similarly for W_e . $V_{u,1}$ contains the 5% of singular vectors with largest singular values, $V_{u,2}$ the next 5%, and so on. Let $V_{u,j:k}$ be the matrix obtained concatenating $[V_{u,j} \dots V_{u,k}]$, and (Fig. 1) let $\Phi_{u,j:k} = V_{u,j:k} V_{u,j:k}^\top$ (similarly for W_e). We can then project any d -dimensional vector onto the U-dark (E-dark) space by multiplying them by $\Phi_{u,20:20}$ (resp. $\Phi_{e,20:20}$).

We form a hierarchy of nested filters $\Phi_{u,1:k}$: multiplying a vector by $\Phi_{u,1:k}$ projects it onto the subspace of the $kd/20$ “least dark” dimensions. We also define filters that combine singular vectors of W_u and W_e (Fig. 5):

$$\Psi_k = (I - \Phi_{e,(k+1):20} \Phi_{u,(k+1):20}), k = 1, \dots, 19 \quad (3)$$

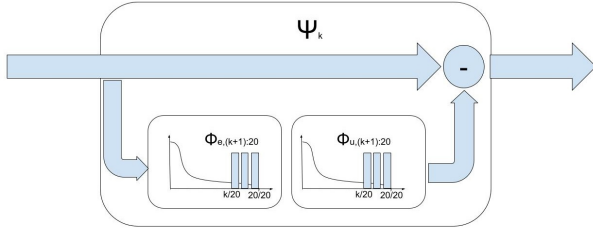


Figure 5 Ψ filters project vectors onto subspaces that are dark according to both the embedding and the unembedding matrix decomposition.

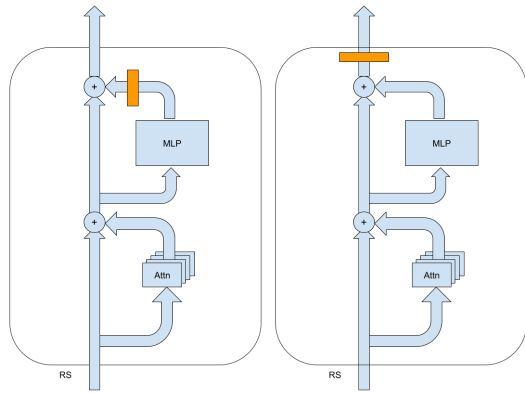


Figure 6 The two positions where we applied spectral filters: on the output of MLP layers, one at a time (left) or on the residual stream after a complete layer (right).

and we set $\Psi_{20} = I$. Multiplying a vector by Ψ_k filters away projections onto subspaces of both W_e and W_u that get darker as k grows. Ψ_{19} filters out only vector components in the 5% dark subspace of *both* W_u and W_e . These definitions make $\Phi_{u,k}$, $\Phi_{e,k}$, and Ψ_k comparable when looking at the fraction of kept/discarded singular projection vectors, although, since it discards a double projection, Ψ_k retains more information. We create a dataset (ccnet-405) of 405 prompts (13,268 tokens) in English, from CCNET (Wenzek et al., 2019). We ran inference on ccnet-405 applying spectral filters to the output of MLP components, one by one (Fig. 6 (left)) and measured the average NLL. We similarly measure NLL when filtering the RS after the contributions of a given target layer have been added to it (Fig. 6 (right)). See App. B for implementation details.

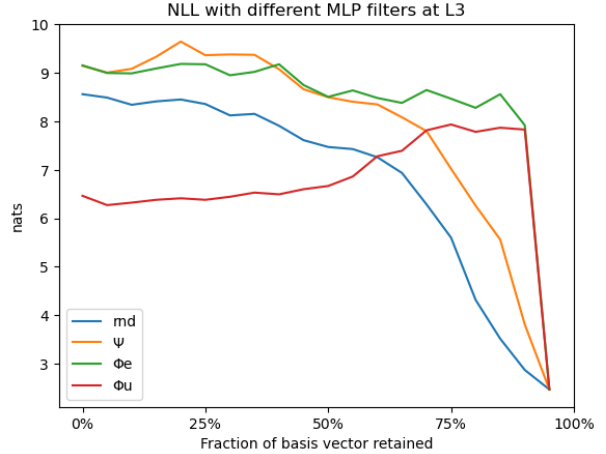


Figure 7 The effect of filtering 13B/L3/MLP with the filters defined in Section 4. ‘Rnd’ indicates filtering projection on subsets of a random orthonormal basis, for reference.

4.1 Discussion

When filtering MLP layers of LLaMa2 13B, the effects of masking L0 and L3 dwarf all others.

When filtering the output of the MLP at L3 (Fig. 7) the loss remains poor until the last 5% of the spectrum is included for both the Φ spectral filters. The fact that the Ψ curve is always above the random filter indicates that this MLP exerts strong influence operating in the dark subspace. See Appendix C for a discussion of 13B/L0/MLP.

Figure 17 in App. C shows that MLP components with a similar propensity for writing dark signals exist also in LLaMa2 7B (L1) and 70B (L2 and L8).

We also look at what happens to the negative log-likelihood when filtering the residual stream after a given layer (Figures 6 (right) and 8). Even a mild bottleneck after L3 results in a significant increase in NLL, in line with the observation that the MLP in L3 writes in the dark space. If we filter only signals that are dark to both W_e and W_u (Fig. 8(b)), we see bottlenecks continuing to be more harmful than random direction removal (Fig.8(a)) up until L20-25.

Dark signals exist and play an important role in achieving low perplexity, but what is this role?

5 Attention sinks

Xiao et al. (2023) describe *attention sinks*: the special Beginning of Sentence (BoS) ‘Token 0’ receives

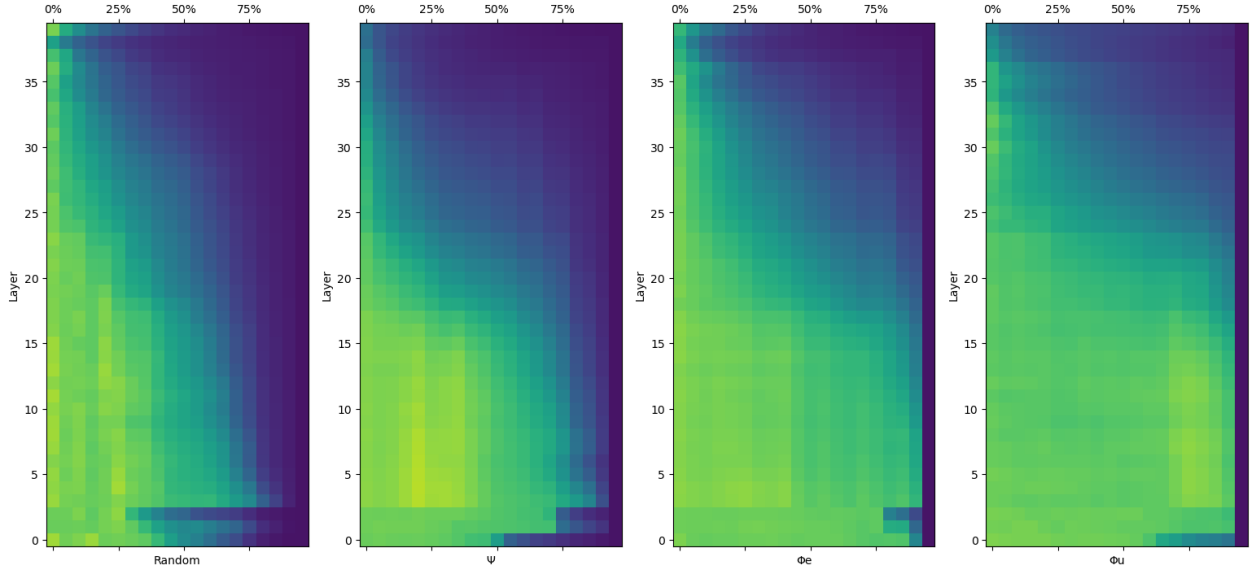


Figure 8 NLL of LLaMa2 13B on ccnet-405 when filtering the residual stream after a given layer (Y-axis), retaining an increasing number of SVs (X-axis) of (c) W_e or (d) W_u . (b) filters from the residual stream only its double projection onto both the W_e and W_u dark spaces. (a) shows, for comparison, the effect of adding more and more dimension in a random orthogonal base. See Fig.19 for similar heatmaps for LLaMa2 7B and 70B.

a disproportionate amount of attention.³ This happens because often an attention head should not be activated in a given context, but the normalisation in the attention scores forces a constant amount of attention to be distributed to previous tokens. The model therefore learns to sink excess attention by allocating it to the BoS token. Since attention heads map content from the residual stream being attended to that of the present token, the content imported when sinking attention should interfere as little as possible with the probability distribution of the next token.

Figure 9 shows how the norm of the Token 0 residual stream progresses over layers, and the contributions from MLPs and MHAs components. We plot the overall norm, and the norms of the projection on the U-Dark space and of the projection on its orthogonal complement (*U-Light*).

After an initial phase of input enrichment that apparently does not need an attention sink, the MLP at L3 blasts off a vector of large norm and almost completely U-dark. This vector acts as an attention collector for heads in need of a sink, and is kept around until the last few layers, where the combined action of MLPs and attention heads first erases it and then replaces it with the vector that encodes the

³Xiao et al. (2023) include the first four tokens in their operational definition of attention sinks, for achieving effective streaming decoding. In our observations the BoS token is by far the one attracting the most attention.

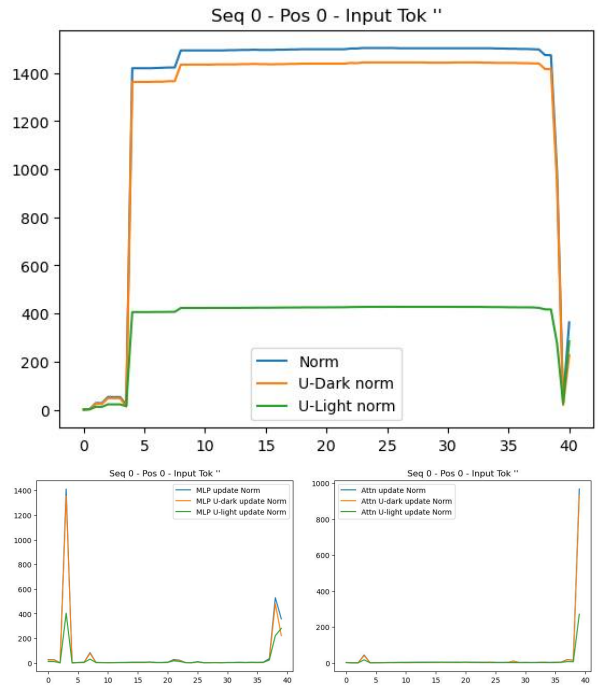


Figure 9 (Top) The composition of the RS of the BoS token for LLaMa2 13B as a function of the layer. (Bottom left) The norms of the contribution of MLP layers to the BoS RS. (Bottom right) The norms of the contribution of Multi-Head Attention components to the BoS RS.

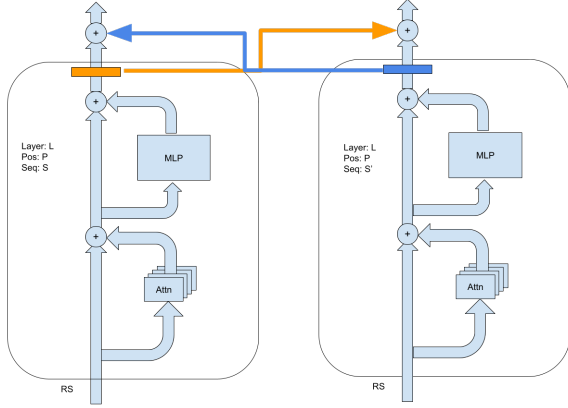


Figure 10 Shavings swap experiment: rather than being suppressed, the subspaces blocked by spectral filters are swapped with the corresponding ones from a token at the same position but in a different sample. This swap perturbs all residual streams except the one for Token 0, since this is identical for all samples due to the autoregressive nature of the model.

probability distribution of the model over generation-initial tokens.

We confirmed that dark signals are primarily used to sink attention with an additional experiment (Fig. 10). We apply spectral filters at the exit of a layer but, rather than suppressing the filtered component, we add it into the corresponding residual stream of a different sample, at the same token position and layer. Since the content of the RS of the BoS is the same irrespective of the input, this procedure leaves it intact, while perturbing all other RSs.

The resulting NLL heatmap is in Fig. 11 (left). Unlike in those in Fig. 8, there is no step-decrease in NLL when the last 5% of singular vectors is added. Conversely, if we apply spectral filters *only* to Token 0, the step-decrease is clearly visible (Fig. 11 (middle)). We conclude therefore that the primary function of the dark subspace is to enable the crucial attention sink mechanism.

6 Sink-preserving spectral filters

The finding that dark signals are essential to enable attention sinks leads to the following question: what would be the impact of spectral filters that preserve dark signals but filter away one or more bands before them? Let $\Omega_{u,k}$ be a new family of spectral filters (Fig. 12):

$$\Omega_{u,k} = ([V_{u,1:k}; V_{u,20:20}])([V_{u,1:k}; V_{u,20:20}])^\top \quad (4)$$

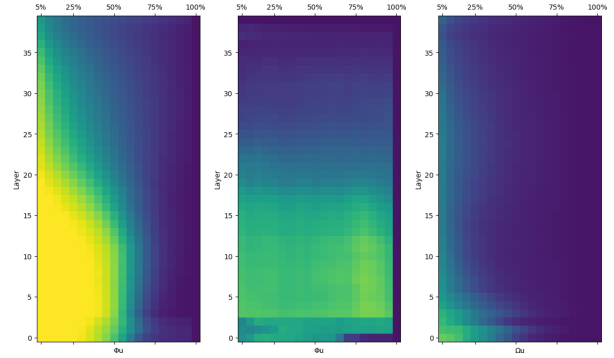


Figure 11 NLL of LLaMa2 13B on ccnet-405 when filtering the residual stream after a given layer (Y-axis). (Left:) Swapping the filtered vector components between RS at the same layer and token position, but in a different sample, perturbing all RSs except the BoS one. (Middle:) Filtering only the residual stream of the BoS token. (Right:) Applying the sink-preserving spectral filters $\Omega_{u,k}$ to a section of the residual stream of LLaMa2 13B right after a layer.

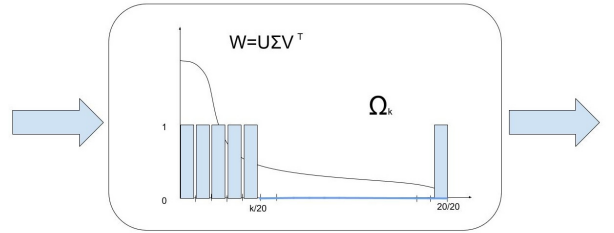


Figure 12 Ω filters project vectors on the head of the spectrum, but also on the tail end to preserve attention sinking.

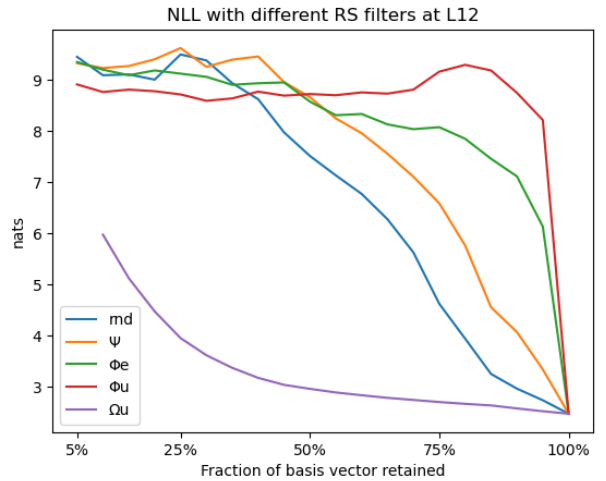


Figure 13 NLL by number of retained dimensions when applying different spectral filters at L12.

<p>Prompt: If you're interested in Grizzly Bear viewing in and around the northern Gulf of Alaska, consider a chartered flight with Trygg Air Alaska based out of King Salmon with service to and from Anchorage.</p>
<p>Ψ(90%): The EA, a GS, the E, A, for a total, the GS, the E, the S, the E, the S, the 15, the 16, the 15, the 16, the 15, the 17, the</p>
<p>Rnd (90%): What is the most beautiful thing that has ever been? What is the most beautiful thing that has ever been? It is not about the most beautiful thing that has ever been. The most beautiful thing that has ever been. It is not about the most beautiful thing that has ever been. It is not</p>
<p>Ω_u (90%): The Grizzly Bear is one of the largest land carnivores in the world. Males can reach a weight of 800 pounds and females can reach a weight of 400 pounds. The Grizzly Bear is one of the most powerful predators in North America</p>

Table 2 Sample generations by LLaMa2 13B with spectral filters applied right after L3.

Fig. 11 (right) shows that low values of NLL are achieved even when masking a significant number of components. As an example (Fig. 13) NLL grows only from 2.47 to 2.74 when suppressing 25% of the SVs by applying $\Omega_{u,14}$ after L12. We validated these results by repeating the experiment with a sample of code from the DeepMind Code Contest dataset (Li et al., 2022) consisting of 117 prompts (14,641 tokens), Fig. 20, and with LLaMa2 7B and 70B (Fig. 19).

6.1 The effect of inhibiting attention sinks on generation quality

So far we have looked at the effect of spectral filters on the negative log-likelihood of prefixes that were fed as prompts to our models. It is interesting to also observe the impact on generated continuations when applying these same filters.

Layers 2-4 are the most fragile to random and Ψ filtering (Tab. 2), while generations remain coherent with Ω filtering irrespective of where the filter is applied, when 10-20% of the singular vectors are suppressed. We notice that the application of Ψ filters often results in the model entering repetitive patterns. This is consistent with the possibility that attention heads largely copy representations from the RSs of previous tokens, and inhibiting attention sinking results in over-copying. More examples can be found in App. D.

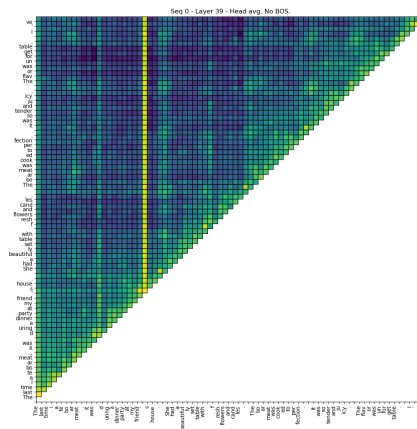


Figure 14 Attention matrix at L39 averaged across heads for a sample. Brighter columns correspond to tokens that are attended by many following tokens (LLaMa2 13B, Token 0 is removed for readability).

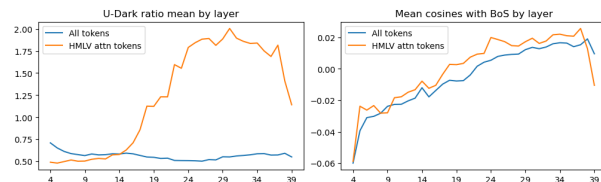


Figure 15 Mean U-Dark ratio (left) and cosine similarity with the BoS RS (right) for high-mean low-variance attention tokens and across all tokens, by layer.

7 Dark Signals and Attention Bars

Inspecting attention matrices in our sample we see that there are frequently a few tokens that also receive a large amount of attention, giving rise to characteristic *attention bars* (e.g. Fig. 14). We hypothesized that such bars could correspond to tokens whose residual streams are similar to that of Token 0, and therefore become additional attention sinks.

We define High-Mean Low-Variance (HMLV) token-layer pairs those with mean received attention over over subsequent tokens above $\tau_\mu = .018$ and variance below $\tau_\sigma = .01$. We ignore layers 0-3, since the attention sink is not in place yet, the BoS token, and the last 4 tokens of each sequence. This heuristic yields 12,236 HMLV token-layer pairs for LLaMa2 13B on ccnet-405 out of a total of 404,748 token-layer pairs for the same tokens and layers considered. We selected threshold manually so that most HMLV tokens appear as “attention bars” in attention matrices.

We define the U-Dark ratio as a measure of the prevalence of U-Dark signals in a representation:

$$udr(h_t^l) = \frac{\|\Phi_{u,20:20}h_t^l\|}{\|(I - \Phi_{u,20:20})h_t^l\|} \quad (5)$$

i.e. the norm ratio between the projection of the residual stream onto the U-dark space, and the projection on its orthogonal complement.

We measured average U-Dark ratio and cosine similarity with the BoS RS for HMLVs, and contrasted them with the same statistics taken over all token-layer pairs. Results are in Fig. 15.

Starting around L13 the U-Dark ratio of HMLVs grows considerably, whereas it remains constantly below .75 for the overall population. At the same time, however, these tokens have cosine similarity with the BoS residual stream largely indistinguishable from the overall distribution, and close to zero. These results neither confirm nor invalidate the hypotheses that attention bars are auxiliary attention sinks. They seem to indicate that they occupy a different subspace *within the dark subspace* from the BoS token, but they may still be attention sinks.

8 Related work

In this work we adopt the framework introduced in (Elhage et al., 2021), which highlights the central role played by the residual stream as working memory and communication channel across components, and hints at the notion of subspaces with differentiated functions. The *logit lens* was first introduced by (Nostalgebraist), and has been since used and extended in a number of interpretation studies, including (Dar et al., 2022; Geva et al., 2022; Belrose et al., 2023; Din et al., 2023; Katz and Belinkov, 2023; Voita et al., 2023). Of these, Dar et al. (2022) analyse models projecting parameter matrices onto the vocabulary space, an approach we are also following in Section 3.

Our hypothesis that the subspace most orthogonal to the vocabulary representation could encode non-sparse latent features that should not interfere with the distribution over the immediate next token appeared supported by (Elhage et al., 2022), where they show that, in basic models, important non-sparse features tend to be assigned principal components rather than being in superposition with sparse features. (Sharkey et al., 2022) showed that sparse autoencoders can recover a ground-truth assignment of features to linear subspaces by means of sparse autoencoders in an artificial and simplified setting and a 31M parameter LLM, with $d = 256$; (Cunningham et al., 2023) apply a similar method to larger Pythia

70M and Pythia 410M models. Our results with Ω filters with the much larger LLaMa2 models indicate that the residual stream could be used at less than full capacity, at least for some of the layers, raising the question of what model of superposition would best apply to them.

The concept of *Attention Sinks* was introduced by Xiao et al. (2023), who noticed that performance of streaming models dropped abruptly once the first tokens moved out of the attention sliding window context. We take here the next step in explaining how this process works, showing how it happens thanks to a very limited and specific portion of the spectrum.

Sharma et al. (2023) show that it is possible to preserve and even improve the performance of the GPT-J (Wang and Komatsuzaki, 2021) model while dropping large portions of component matrices based on the SVD decomposition of the matrices themselves. We also focus on spectral decomposition, but using the spectrum of the unembedding matrix, in accordance with the logit lens approach and the intuition that it represents a common ground for all the components in a model.

9 Conclusions and Future work

A better understanding of the inner workings of transformer models is important to find strategies to make them safer. In this work we explored a novel way to look at transformers, extending the *logit lens* approach into *logit spectroscopy* by introducing *spectral filters*. We explored the hypothesis that dark signals could be used to maintain global features while minimizing their interference with the next token, but we discovered that the main role of dark signals is as collectors for heads in need of an attention sink. We reconstructed how attention sinking works in LLaMa2 models, and we showed that, as long as attention sinking is preserved, they still achieve low loss even when significant portions of the unembedding spectrum are suppressed. Finally, we found a positive correlation between the attention received by a token and the relative prevalence of dark signals in its residual stream, especially in the upper layers.

The results on spectral filtering with dark signal preservation, combined with the observation that transformers are invariant to basis changes in the residual stream, suggest that it could be possible to first "canonicalize" a model so that its residual stream dimensions match the V_u columns, and then compress away from components dimensions that are low in the spectrum but are not used for attention sinking.

We consider such a form of *spectral compression* an interesting direction for future work.

Finally, our exploration of the connection between “attention bars”, prevalence of dark signals, and similarity with the Token 0 residual stream did not give a definite answer to the question of whether attention bars are additional attention sinks or have some other function. Increasing the granularity of the spectral bands in the dark subspace is a promising approach to solve this puzzle.

10 Limitations

We limited our attention to the LLaMa2 family of models, and only to the pretrained models prior to their instruction and safety fine-tuning. It is possible that other models do not realise attention sinks in the same way, or that they might not need them.⁴

The number of conditions tested in our detailed spectral filtering experiments meant that we could use only a text sample of limited size. While we did repeat some of the experiments using a code sample, we cannot exclude that there could be some differences when using samples from drastically different distributions, e.g. in languages using different scripts.

11 Ethical Considerations

While our aim in studying the behaviour of LLMs is to make them more transparent, controllable, and trustworthy, it is conceivable that increased understanding could also benefit malicious agents intending to undertake harmful actions. Besides this generic considerations, we cannot see problematic ethical issues arising from this work.

Acknowledgements

We thank the Transparent LLM team of Meta, in particular Lena Voita, Yihong Chen, Javier Ferrando, and Karen Hambardzumyan, for important suggestions and insightful discussions.

References

Nora Belrose, Zach Furman, Logan Smith, Danny Halawi, Igor Ostrovsky, Lev McKinney, Stella Biderman, and Jacob Steinhardt. Eliciting latent predictions from transformers with the tuned lens. *arXiv preprint arXiv:2303.08112*, 2023.

⁴For example by using *off by one softmax* Miller.

Hoagy Cunningham, Aidan Ewart, Logan Riggs, Robert Huben, and Lee Sharkey. Sparse autoencoders find highly interpretable features in language models. *arXiv preprint arXiv:2309.08600*, 2023.

Guy Dar, Mor Geva, Ankit Gupta, and Jonathan Berant. Analyzing transformers in embedding space. *arXiv preprint arXiv:2209.02535*, 2022.

Alexander Yom Din, Taelin Karidi, Leshem Choshen, and Mor Geva. Jump to conclusions: Short-cutting transformers with linear transformations. *arXiv preprint arXiv:2303.09435*, 2023.

Nelson Elhage, Neel Nanda, Catherine Olsson, Tom Henighan, Nicholas Joseph, Ben Mann, Amanda Askell, Yuntao Bai, Anna Chen, Tom Conerly, Nova DasSarma, Dawn Drain, Deep Ganguli, Zac Hatfield-Dodds, Danny Hernandez, Andy Jones, Jackson Kernion, Liane Lovitt, Kamal Ndousse, Dario Amodei, Tom Brown, Jack Clark, Jared Kaplan, Sam McCandlish, and Chris Olah. A mathematical framework for transformer circuits. *Transformer Circuits Thread*, 2021. <https://transformer-circuits.pub/2021/framework/index.html>.

Nelson Elhage, Tristan Hume, Catherine Olsson, Nicholas Schiefer, Tom Henighan, Shauna Kravec, Zac Hatfield-Dodds, Robert Lasenby, Dawn Drain, Carol Chen, Roger Grosse, Sam McCandlish, Jared Kaplan, Dario Amodei, Martin Wattenberg, and Christopher Olah. Toy models of superposition. *Transformer Circuits Thread*, 2022. https://transformer-circuits.pub/2022/toy_model/index.html.

Mor Geva, Roei Schuster, Jonathan Berant, and Omer Levy. Transformer feed-forward layers are key-value memories. *arXiv preprint arXiv:2012.14913*, 2020.

Mor Geva, Avi Caciularu, Kevin Ro Wang, and Yoav Goldberg. Transformer feed-forward layers build predictions by promoting concepts in the vocabulary space. *arXiv preprint arXiv:2203.14680*, 2022.

Shahar Katz and Yonatan Belinkov. Interpreting transformer’s attention dynamic memory and visualizing the semantic information flow of gpt. *arXiv preprint arXiv:2305.13417*, 2023.

Yujia Li, David Choi, Junyoung Chung, Nate Kushman, Julian Schrittwieser, Rémi Leblond, Tom Eccles, James Keeling, Felix Gimeno, Agustin Dal Lago, Thomas Hubert, Peter Choy, Cyprien de Masson d’Autume, Igor Babuschkin, Xinyun Chen, Po-Sen Huang, Johannes Welbl, Sven Gowal, Alexey Cherepanov, James Molloy, Daniel J. Mankowitz, Esme Sutherland Robson, Pushmeet Kohli, Nando de Freitas, Koray Kavukcuoglu, and Oriol Vinyals. Competition-level code generation with alphacode. *Science*, 378(6624):1092–1097, 2022. doi: 10.1126/science.abq1158. <https://www.science.org/doi/abs/10.1126/science.abq1158>.

Kevin Meng, David Bau, Alex Andonian, and Yonatan Belinkov. Locating and editing factual associations

- in gpt. *Advances in Neural Information Processing Systems*, 35:17359–17372, 2022.
- Evan Miller. Attention is off by one. <https://www.evanmiller.org/attention-is-off-by-one.html>. <https://www.evanmiller.org/attention-is-off-by-one.html>.
- Nostalgebraist. interpreting gpt: the logit lens. <https://www.alignmentforum.org/posts/AcKRB8wDpdaN6v6ru/interpreting-gpt-the-logit-lens>.
- Catherine Olsson, Nelson Elhage, Neel Nanda, Nicholas Joseph, Nova DasSarma, Tom Henighan, Ben Mann, Amanda Askell, Yuntao Bai, Anna Chen, Tom Conerly, Dawn Drain, Deep Ganguli, Zac Hatfield-Dodds, Danny Hernandez, Scott Johnston, Andy Jones, Jackson Kernion, Liane Lovitt, Kamal Ndousse, Dario Amodei, Tom Brown, Jack Clark, Jared Kaplan, Sam McCandlish, and Chris Olah. In-context learning and induction heads. *Transformer Circuits Thread*, 2022. <https://transformer-circuits.pub/2022/in-context-learning-and-induction-heads/index.html>.
- Tiago Pimentel, Josef Valvoda, Rowan H Maudslay, Ran Zmigrod, Adina Williams, and Ryan Cotterell. Information-theoretic probing for linguistic structure. In *Proceedings of the 58th Annual Meeting of the Association for Computational Linguistics*, pages 4609–4622. Association for Computational Linguistics, 2020.
- Lee Sharkey, Dan Braun, and Beren Millidge. Taking features out of superposition with sparse autoencoders. In *AI Alignment Forum*, 2022.
- Pratyusha Sharma, Jordan T Ash, and Dipendra Misra. The truth is in there: Improving reasoning in language models with layer-selective rank reduction. *arXiv preprint arXiv:2312.13558*, 2023.
- Noam Shazeer. Glu variants improve transformer. *arXiv preprint arXiv:2002.05202*, 2020.
- Jianlin Su, Murtadha Ahmed, Yu Lu, Shengfeng Pan, Wen Bo, and Yunfeng Liu. Roformer: Enhanced transformer with rotary position embedding. *Neurocomputing*, page 127063, 2023.
- Eric Todd, Millicent L Li, Arnab Sen Sharma, Aaron Mueller, Byron C Wallace, and David Bau. Function vectors in large language models. *arXiv preprint arXiv:2310.15213*, 2023.
- Hugo Touvron, Louis Martin, Kevin Stone, Peter Albert, Amjad Almahairi, Yasmine Babaei, Nikolay Bashlykov, Soumya Batra, Prajjwal Bhargava, Shruti Bhosale, et al. Llama 2: Open foundation and fine-tuned chat models. *arXiv preprint arXiv:2307.09288*, 2023.
- Ashish Vaswani, Noam Shazeer, Niki Parmar, Jakob Uszkoreit, Llion Jones, Aidan N Gomez, Łukasz Kaiser, and Illia Polosukhin. Attention is all you need. *Advances in neural information processing systems*, 30, 2017.
- Elena Voita and Ivan Titov. Information-theoretic probing with minimum description length. In *Proceedings of the 2020 Conference on Empirical Methods in Natural Language Processing (EMNLP)*, pages 183–196, 2020.
- Elena Voita, David Talbot, Fedor Moiseev, Rico Sennrich, and Ivan Titov. Analyzing multi-head self-attention: Specialized heads do the heavy lifting, the rest can be pruned. *arXiv preprint arXiv:1905.09418*, 2019.
- Elena Voita, Javier Ferrando, and Christoforos Nalmpantis. Neurons in large language models: Dead, n-gram, positional. *arXiv preprint arXiv:2309.04827*, 2023.
- Ben Wang and Aran Komatsuzaki. GPT-J-6B: A 6 Billion Parameter Autoregressive Language Model. <https://github.com/kingoflolz/mesh-transformer-jax>, May 2021.
- Guillaume Wenzek, Marie-Anne Lachaux, Alexis Conneau, Vishrav Chaudhary, Francisco Guzmán, Armand Joulin, and Edouard Grave. Ccnet: Extracting high quality monolingual datasets from web crawl data. *arXiv preprint arXiv:1911.00359*, 2019.
- Guangxuan Xiao, Yuandong Tian, Beidi Chen, Song Han, and Mike Lewis. Efficient streaming language models with attention sinks. *arXiv preprint arXiv:2309.17453*, 2023.
- Biao Zhang and Rico Sennrich. Root mean square layer normalization. *Advances in Neural Information Processing Systems*, 32, 2019.

Appendix

D Generation examples

A Notation

Table 3 summarizes the notation used throughout the paper.

B Implementation details

Spectral filtering experiments were run on servers with up to 8 NVIDIA A100 GPUs, each with 80GB of memory, and were implemented modifying the public Llama code from <https://github.com/facebookresearch/llama>. Inference used nucleus sampling with the default parameters ($\text{top-p} = .9$, $T = .6$). Each heat-map took up to 4 hours to complete (for the 70B models).

C Additional spectral filtering experiments

When filtering the output of the MLP of LLaMa2 13B at L0 with filters $\Phi_{e,1:k}$ log-likelihood remains poor (around 9) (Fig.16) until about 90% of W_e 's RSVs are retained. This indicates that the MLP in L0 exerts its effect by writing mostly into an E-dark subspace. The fact that the NLL recovers steadily starting from when about 40% of the RSVs of W_u are retained, and that the curve for the Ψ_k filters is close to the random masking, show that this MLP writes mostly in the target unembedding space.

Figure 17 plots the NLL loss when applying spectral filters to the MLP at L1 in LLaMa2 7B, and at L2 and L8 in LLaMa2 70B. The loss profiles of component 7B/L1/MLP (left) are similar to those of 13B/L3/MLP: it exerts its influence in a subspace that is dark to both embeddings and unembeddings, and indeed it is the MLP that creates the attention sink vector in the Token 0 residual stream. 70B/L2/MLP and 70B/L8/MLP are the components responsible for the attention sink in 70b (Fig. 18). Unlike with 7B and 13B, the attention sink vector in Token 0 is U-Dark but not E-Dark, and is formed in two steps at L2 and L8.

Figure 19 shows NLL loss heat-maps for LLaMa2 7B (top) and 70B (bottom) when spectral filters are applied to the RS at the layer on the Y axis.

Figure 20 displays similar heat-maps for LLaMa2 13B, using a sample of code fragments from the solutions of the DeepMind Code Contest dataset rather than cnet-405.

V	Vocabulary
$L\langle X \rangle$	Layer X
$H\langle Y \rangle$	Head Y
d	Model dimension
d_h	Head dimension
d_m	MLP hidden layer dimension
$h_t^l \in \mathcal{R}^d$	Intermediate repr. for Token t at layer l
$W_z, z \in \{1, 2, 3\}$	MLP matrices ($W_1, W_3 \in \mathcal{R}^{d \times d_m}$), $W_2 \in \mathcal{R}^{d_m \times d}$
$W_z, z \in \{k, q, v, o\}$	Attention matrices ($W_q, W_k, W_v \in \mathcal{R}^{d \times d_h}$, $W_o \in \mathcal{R}^{d_h \times d}$)
$W_z, z \in \{e, u\}$	Embeddings and unembeddings ($\in \mathcal{R}^{ V \times d}$)
$V_y, y \in \{e, u\}$	right singular vectors of emb. and unemb. matrices

Table 3 Notation for referring to model components.

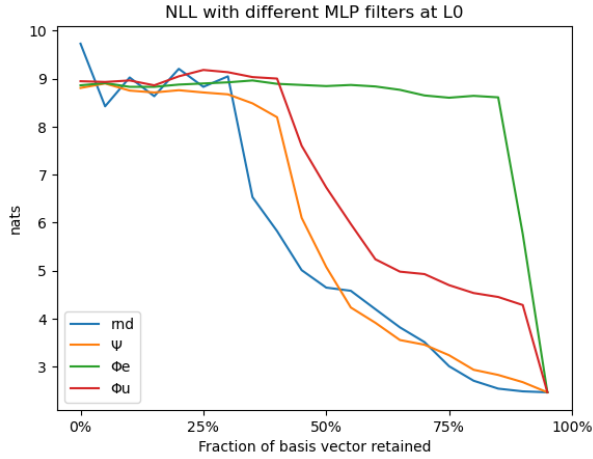


Figure 16 The effect of filtering 13B/L0/MLP with the filters defined in Section 4.

Prompt: By Bart B. Van Bockstaele Mar 19, 2009 in Science			
	Ψ (95%)	Rnd (95%)	Ω_u (95%)
L0	In this paper, we will discuss the differences between the currently most popularly used programming languages, C, C++, C#, and Java. We will also discuss the advantages and disadvantages of each programming language. C is the oldest programming language of the four. C was developed by Dennis Ritchie in	A team of scientists from the University of Alberta, Canada, has discovered a new species of dinosaur. The new species is called Borealopelta markmitchelli. The scientists say that it is a close relative of the famous armored dinosaur Ankylosaurus.	In a recent study, researchers at the University of California, Riverside have found that the presence of an endocrine-disrupting chemical in the environment can alter the behavior of male fruit flies in a way that increases their chances of mating. The chemical in question is called meth
L2	The most important thing is to find out how to get a good grip on the bart is the most important thing in the world. The bart is the most important thing in the world. the bart is the most important thing in the world. the bart is the most important thing in the world.	The giant planets Jupiter and Saturn are being observed by the Cassini spacecraft in the solar system. The images are showing the planets and their moons in a way that has never been seen before. The Cassini spacecraft is currently orbiting the planet Saturn, which it has been doing	A team of scientists from the University of California, San Diego, have discovered that a protein in the human body that is known to play a role in the progression of Parkinson's disease may also be a factor in the development of autism. The researchers have found that mutations in the protein
L3	Van Bostis, 1969, 1969, 1969, 1969, 1969, 1969, 1969, 196	By Bart B. Van Bockstaele Mar 19, 2009 in Science By Bart B. Van Bockstaele Mar 19, 2009 By Bart B. Van Bockstaele In the context of the current discussions on the future of the EU and the European Union, I would like to draw your attention to the following:	A new study by researchers at the University of California at San Francisco suggests that the use of acupuncture may actually reduce the risk of miscarriage. The study was based on data from 1,417 women who were pregnant and were treated at the San Francisco General Hospital between
L12	The chemicals that make the brain think and the body work are the same ones that make the world go around, and the same ones that make the world go wrong. The universe is the great unknown, and it is a great unknown because it is the great unknown. The universe is a big place, and	A new study has found that a certain species of fish is able to survive in the most polluted waters of the world. The study, conducted by researchers from the University of Guelph, found that the fathead minnow, which is a small fish found in the Great Lakes, can surv	In a recent press release, the University of Leicester announced that its researchers have discovered a new way to get to the heart of the matter, literally. The researchers at the University of Leicester have discovered a new way to get to the heart of the matter, literally. The researchers
L32	The oldest known animal to have ever lived on Earth, a 530-million-year-old sea creature, has been discovered in the Canadian Arctic. The creature, a 10-centimeter (3.9-inch) long worm, has been named the Hallucigenia	The "green" and "sustainable" movement is gaining momentum in the U.S. and around the world. The latest development is the Sustainable Urbanism conference in San Francisco, California. The "green" and "sustainable" movement is gaining momentum in the	The European Space Agency (ESA) is sending the first European astronaut into space since 1998. The mission is scheduled for the end of April. The ESA is sending the first European astronaut into space since 1998. The mission is scheduled for the end of April.
L38	The discovery of a new species of bird in the Philippines has been announced by scientists from the Field Museum in Chicago. The new bird is called the Visayan warty pig, or the Visayan bleeding-heart pigeon. It was found on the island of Dinagat in	The European Space Agency (ESA) has released the first images of the 1323-pound (600 kg) GOCE satellite in orbit. The satellite is designed to map Earth's gravitational field with unprecedented accuracy. GOCE, or Gravity field and steady	The "Higgs boson" is the "God particle" that is needed to make the Standard Model complete. It has been missing for decades, but now the search is on in earnest. The Standard Model is a theory of elementary particles and their interactions. The model is based on the idea that

Table 4 Generations from LLaMa2 13B with Residual Stream filtered at one layer, comparing removing 5% random projections, Ψ filtering, and Ω_u filtering. Note that generations can be a mixture of true (but most likely never written by the author in the prompt) and hallucinated content.

Prompt: If you're interested in Grizzly Bear viewing in and around the northern Gulf of Alaska, consider a chartered flight with Trygg Air Alaska based out of King Salmon with service to and from Anchorage.			
	Ψ (90%)	Rnd (90%)	Ω_u (90%)
L0	Trygg Air Alaska is a small air taxi company based in King Salmon, Alaska. The company provides chartered flights from King Salmon to Anchorage, Alaska, which is the nearest city to King Salmon with an airport. The company is owned by a man named Try	The Alaska Department of Fish and Game (ADFG) has been conducting an aerial survey of the Gulf of Alaska for Grizzly Bears since 2006. The survey is conducted each summer to estimate the number of bears in the Gulf. The survey area covers	The flight is a one-hour scenic trip that flies over the Alaska Peninsula and Bristol Bay. You'll be able to view the Alaskan wilderness and Grizzly Bears in their natural habitat. The flight includes a stop at the Brooks Camp for a
L3	The EA, a GS, the E, A, for a total, the GS, the E, the S, the E, the S, the 15, the 16, the 15, the 16, the 15, the 17, the	What is the most beautiful thing that has ever been? What is the most beautiful thing that has ever been? It is not about the most beautiful thing that has ever been. The most beautiful thing that has ever been. It is not about the most beautiful thing that has ever been. It is not	The Grizzly Bear is one of the largest land carnivores in the world. Males can reach a weight of 800 pounds and females can reach a weight of 400 pounds. The Grizzly Bear is one of the most powerful predators in North America
L4	The ACS, or, the A.S.E. The A.S.S.A.S. on the E.S.A. The A.S.E.E.A.S. on the E.S.A. The A.S.S.A	The Grizzly Bear is a wild creature and not a domesticated pet, so when you're dealing with a wild creature, you have to be careful with your approach and how you do it. The Grizzly Bear is a wild creature and not a domesticated pet, so when you'	Trygg Air Alaska is a family owned and operated air service based out of King Salmon, Alaska. We offer flightseeing tours and charter services to the Alaska Peninsula, Bristol Bay, and the Aleutian Islands. We have been flying in the region since 19
L6	The cost is about \$1,500 per person, but the trip is about a month long. The Gulf of Alaska is the only place in the world the bears are a problem. The trip is the same, but the bears are not. The bears are the same	Trygg Air Alaska is a charter service offering air transportation between Anchorage, Alaska and King Salmon, Alaska. With a fleet of two Piper Cherokee 6 aircraft, Trygg Air Alaska offers an economical alternative to commercial airlines and private aircraft. The	Trygg Air Alaska is a small air charter service based out of King Salmon, Alaska. They provide flight services to and from Anchorage and the remote communities of King Salmon, Iliamna, and Bristol Bay. Trygg Air Alaska offers a range of services, including scen
L10	The Tail, the Beings, and the Salmon The Tail, the Beings, and the Salmon The Tail, the Beings, and the Salmon The Tail, the Beings, and the Salmon	Trygg Air Alaska is a family owned business, with the same values as our Alaskan ancestors: honesty, integrity and hard work. We've been in the air since 2010 and we've flown more than 500,000 miles over the beautiful	Trygg Air Alaska is a family owned and operated airline based in King Salmon, Alaska. Trygg Air Alaska has been providing charter services to the Grizzly Bear Viewing lodges in and around the Gulf of Alaska since 1989. We have the
L22	A Grizzly Bear viewing charter with Try The best time to see bears is from the end of the first week of the 2018/19 salmon run, through to the end of the 2019/2020 salmon run. The sal	Grizzly Bear viewing is an amazing experience. The bears are beautiful, majestic and awe-inspiring. The bears are also dangerous, and there are a lot of things to consider before you set out to view them. Trygg Air Alaska is dedicated to providing	Grizzly Bear viewing can be arranged in conjunction with fishing trips or as a separate trip. Fly-out trips can be arranged to view the Grizzly Bears at Brooks Falls, McNeil River, Katmai National Park, Lake Clark National Park,
L32	Trygg Air Alaska offers chartered flights for the purpose of viewing grizzly bears in and around the northern Gulf of Alaska. The northern gulf of Alaska is the only place in the world where grizzly bears are known to catch and eat the endanger	Grizzly Bear Viewing from the air The Gulf of Alaska is home to a large population of Grizzly Bears. There are approximately 1000 bears in the area, which is considered one of the largest Grizzly Bear populations in the world. In addition	Grizzly Bear Viewing, Fishing and More. Trygg Air Alaska is a charter air service based out of King Salmon, Alaska. Trygg Air Alaska has been operating for over 20 years. Trygg Air Alaska offers charters to the Katmai National

Table 5 Generations from LLaMa2 13B with Residual Stream filtered at one layer, comparing removing 10% random projections, Ψ filtering, and Ω_u filtering.

Prompt: Tuatara are lizard-like reptiles that can be traced back to the time of the dinosaurs. For the first time in 200 years, researchers have discovered a baby tuatara on mainland New Zealand.			
	Ψ (95%)	Rnd (95%)	Ω_u (95%)
L1	The baby tuatara is a tuatara that is a tuatara	The tuatara is a reptile that is unique to New Zealand and has survived from the time of the dinosaurs. It is the only surviving member of the order Rhynchocephalia. The tuatara was once found throughout the North Island and offshore islands, but	The discovery was made by a team of researchers from the University of Auckland and the Department of Conservation. The team was conducting a survey of tuatara populations on the island of Raoul, when they came across a juvenile tuatara. The tuatara is a species of
L3	The full, 200 year, 1,166,1,1661,1,1,1661, 1,1,1661,1,1,1661,1, 1,1661,1,1,1	Tuatara are lizard-like reptiles that can be traced back to the time of the dinosaurs. For the first time in 200 years, researchers have discovered a baby tuatara on mainland New Zealand. This is the first time since the 1800	Tuatara are a native species to New Zealand, but they are notoriously difficult to breed in captivity. Tuatara are lizard-like reptiles that can be traced back to the time of the dinosaurs. For the first time in 200 years,
L4	The adult is the first time a baby has been found in the world. The first time a baby has been found in the world. The first time a baby has been found in the world. The first time a baby has been found in the world. The first time a baby has been found in the	Tuatara are lizard-like reptiles that can be traced back to the time of the dinosaurs. For the first time in 200 years, researchers have discovered a baby tuatara on mainland New Zealand. The tuatara, which has not yet been	Tuatara are found only in New Zealand, and are the only surviving members of the order Rhynchocephalia, which dates back to the time of the dinosaurs. They can be found on the North, South and Stewart Islands, but the tuatara found on the mainland are
L7	A 2016, the world's population reached the 7.5 billion mark, the same number that now lives on the world, and the same number that now lives on the world, and the same number that now lives on the world, and the same number that now lives on the world,	Tuatara are lizard-like reptiles that can be traced back to the time of the dinosaurs. For the first time in 200 years, researchers have discovered a baby tuatara on mainland New Zealand. The tuatara was found in a rocky	Tuatara are lizard-like reptiles that can be traced back to the time of the dinosaurs. For the first time in 200 years, researchers have discovered a baby tuatara on mainland New Zealand. The tuatara is a reptile that
L10	The last time a live one was found, the world was a different place. The world was at the end of the 1800s, the age of the "1840s, the 1840s, the 1840s, the 184	The tuatara, named Pine, was found on Stephens Island in the Cook Strait, 15 kilometres from the nearest mainland. The tuatara, named Pine, was found on Stephens Island in the Cook Strait, 15 kilometres from the nearest mainland. Ph	The baby tuatara was found on the shore of a lake in the Otago region of New Zealand. Tuatara are a unique species of reptile that is native to New Zealand. They are the only living members of their family, and are closely related to lizards.
L15	The small, 5.5-inch-long, 4-year-old female was found by a group of children at the, "I, or the world, would have to be pretty stupid to think that there weren't more than one," he said. Tuatua is the only	The tuatara was discovered in 2017 at the Karori Wildlife Sanctuary in Wellington, New Zealand. It is the first of its kind to be found in the wild on mainland New Zealand since the 1800s. Tuatara are a species of l	The tuatara is the last remaining member of a reptile order that flourished around 200 million years ago. It has survived for so long because of its slow metabolism, which allows it to survive on a diet of insects, small birds, lizards,
L36	The baby tuatara was discovered on a small island off the North Island. It is believed the tuatara was washed ashore by a storm. The tuatara is the only surviving member of a group of reptiles that lived during the time of the dinosaurs. The	The tuatara is a nocturnal reptile, and it is a lizard-like creature that can be traced back to the time of the dinosaurs. Tuatara are lizard-like reptiles that can be traced back to the time of the dinosaurs	The tuatara is a lizard-like reptile that is endemic to New Zealand. It is the only living member of the order Rhynchocephalia, which flourished in the Triassic and Jurassic periods, and it is the last surviving member of a lineage

Table 6 Generations from LLaMa2 13B with Residual Stream filtered at one layer, comparing removing 5% random projections, Ψ filtering, and Ω_u filtering. Note that generations can be a mixture of true and hallucinated content.

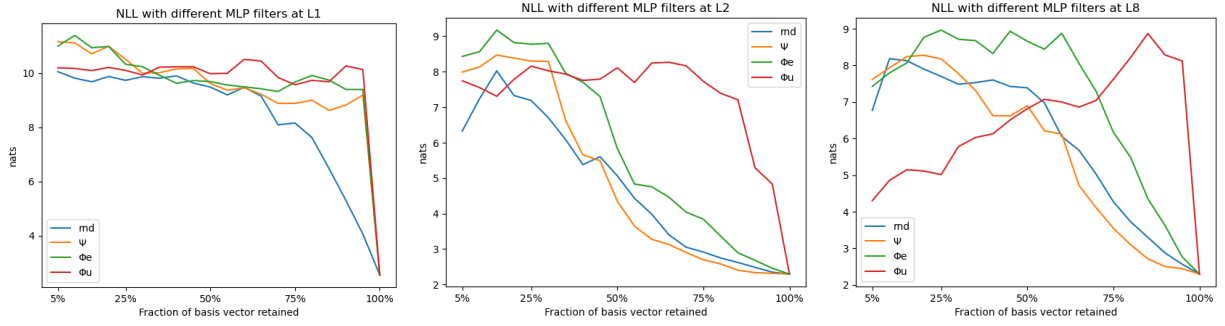


Figure 17 NLL filtering of MLPs in Llama2 7B (left) and 70B (middle) and (right) highlighting layers operating in the dark space.

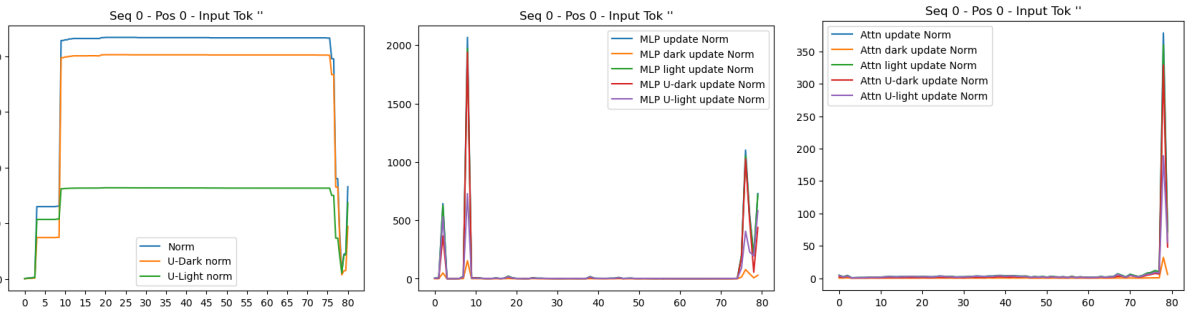


Figure 18 Token 0 residual stream in LLaMa2 70B. (left): RS norms by layer; (middle) norm of MLP contributions; (right) norm of MHA contributions.

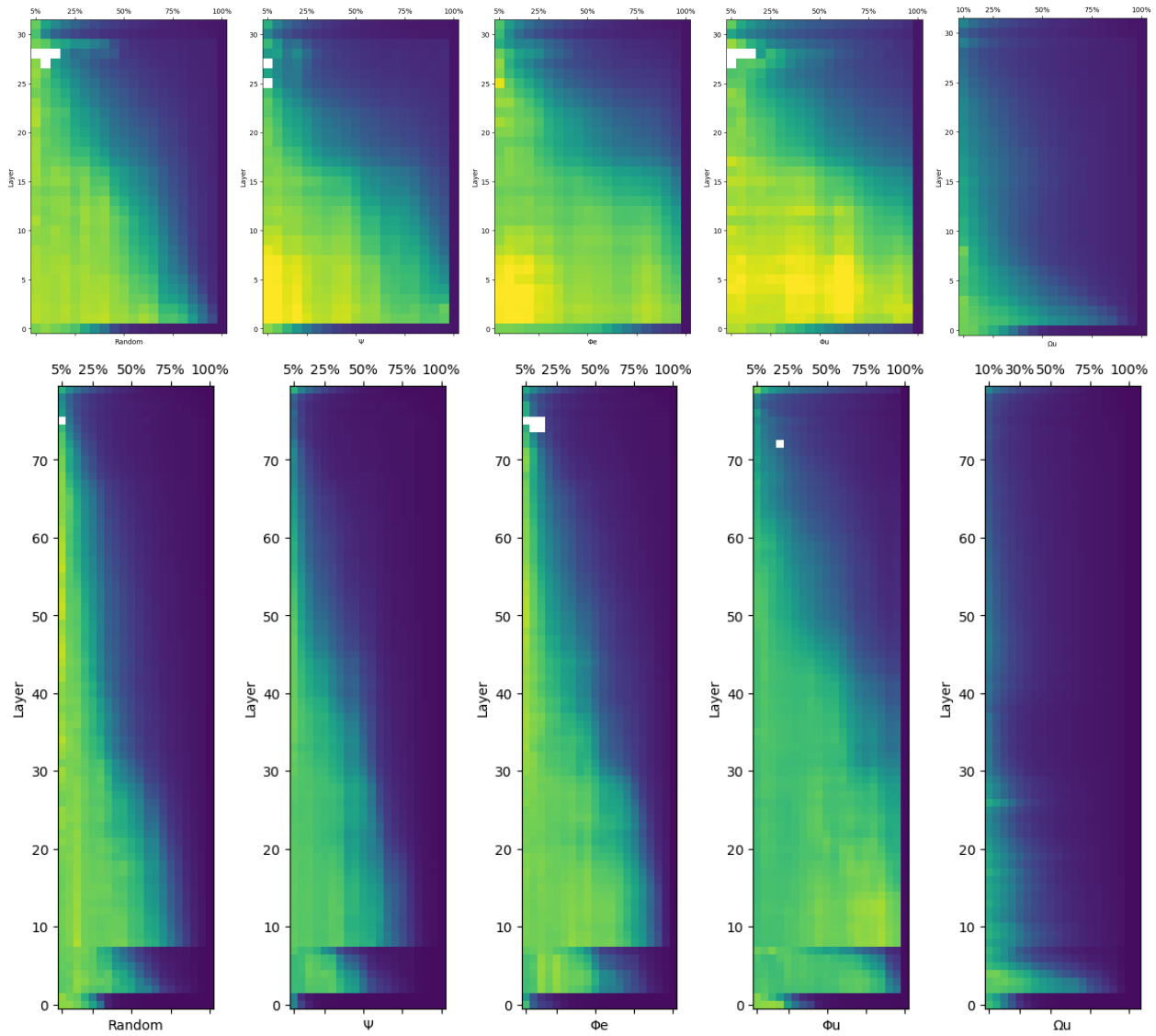


Figure 19 Negative Log-Likelihood when filtering the Residual Stream one layer at a time in LLaMa2 7B (top) and LLaMa2 70B (bottom). White cells correspond to configurations where NLL diverged for at least one of the samples.

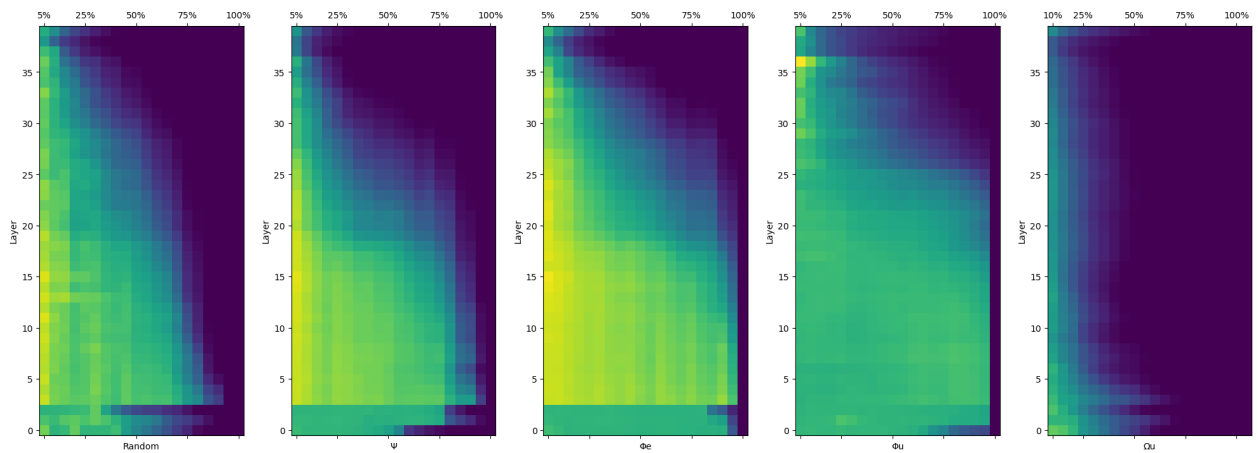


Figure 20 NLL filtering of MLPs in LLaMa2 13B on a sample of code from the DeepMind Code Contest dataset.